Behavioral/Systems/Cognitive

Specialization of Binaural Responses in Ventral Auditory Cortices

Nathan C. Higgins,[1] Douglas A. Storace,[1] Monty A. Escabí,[1,2,3] and Heather L. Read[1,2]

[1]Department of Psychology, Behavioral Neuroscience Division, and Departments of [2]Biomedical Engineering and [3]Electrical Engineering, University of Connecticut, Storrs, Connecticut 06269

Accurate orientation to sound under challenging conditions requires auditory cortex, but it is unclear how spatial attributes of the auditory scene are represented at this level. Current organization schemes follow a functional division whereby dorsal and ventral auditory cortices specialize to encode spatial and object features of sound source, respectively. However, few studies have examined spatial cue sensitivities in ventral cortices to support or reject such schemes. Here Fourier optical imaging was used to quantify best frequency responses and corresponding gradient organization in primary (A1), anterior, posterior, ventral (VAF), and suprarhinal (SRAF) auditory fields of the rat. Spike rate sensitivities to binaural interaural level difference (ILD) and average binaural level cues were probed in A1 and two ventral cortices, VAF and SRAF. Continuous distributions of best ILDs and ILD tuning metrics were observed in all cortices, suggesting this horizontal position cue is well covered. VAF and caudal SRAF in the right cerebral hemisphere responded maximally to midline horizontal position cues, whereas A1 and rostral SRAF responded maximally to ILD cues favoring more eccentric positions in the contralateral sound hemifield. SRAF had the highest incidence of binaural facilitation for ILD cues corresponding to midline positions, supporting current theories that auditory cortices have specialized and hierarchical functional organization.

Introduction

Mammals accurately localize sounds using physical cues that change systematically as a function of where a sound is relative to the body midline (Hartmann, 1999). When sound is displaced to the left, it is reflected off the head and pinna, resulting in lower sound level reaching the right ear. This interaural level difference (ILD) is a primary binaural cue used to determine the horizontal position of sound (Hartmann, 1999). Sound frequency distortions caused by head and pinna reflections cue the vertical position of sound (Musicant and Butler, 1984; Middlebrooks and Green, 1990; Shaw, 1966). When binaural cues are absent and hearing is monaural, as is the case when one ear is plugged or deaf, mammals do not accurately locate sound in vertical or horizontal dimension, underscoring the importance of binaural cues for locating sounds in the acoustic scene (Wightman and Kistler, 1992; Slattery and Middlebrooks, 1994; King et al., 2000; Macpherson and Middlebrooks, 2002).

Auditory cortices are sensitive to sound localization cues and positions in space, but it is not clear whether they are all functionally organized to encode spatial attributes of sound (Semple and Kitzes, 1993a; Recanzone, 2000; Stecker et al., 2003, 2005a; Zhang et al., 2004; Mrsic-Flogel et al., 2005; Campbell et al., 2006b; Harrington et al., 2008; Nelken et al., 2008; Popescu and Polley, 2010). All core and some belt auditory cortices have best frequency (BF) responses to sound that are organized into topographic BF gradients (Reale and Imig, 1980; Recanzone et al., 2000; Lee and Winer, 2008; Hackett, 2010). The cortex is also organized into response gradients and modules that vary in sound intensity and frequency resolution distinct from the BF gradient (Read et al., 2002; Polley et al., 2007). Although BF and sound-intensity cues could indicate position sensitivity (Schnupp et al., 2001; King et al., 2007), they could serve functions independent of localization. Binaural ILD sensitivity is directly related to horizontal sound position sensitivity (Wenstrup et al., 1988; Campbell et al., 2006a,b) and is topographically organized within primary auditory field (A1) (Middlebrooks and Zook, 1983; Irvine and Gago, 1990; Nakamoto et al., 2004), but little is known about its organization within neighboring core and belt cortices. Dual stream hypotheses postulate that higher-level dorsal and ventral parabelt auditory cortices specialize to process "where" versus "what" a sound is, respectively (Recanzone and Cohen, 2010). This dual specialization of parabelt cortices could, in theory, exist initially in dorsal and ventral core and belt cortices that are connected via separate anatomical pathways (Hackett, 2010).

Few studies directly compare response properties between multiple auditory cortical fields, making it difficult to draw strong inferences about large-scale functional organization. Here we take advantage of optical imaging and the small area of cortical fields in the rat to assess binaural ILD response sensitivities in multiple cortices in the same animal. We find ILD cue sensitivity is a ubiquitous organizational feature in A1 and ventral cortical

Received May 17, 2010; revised Aug. 30, 2010; accepted Sept. 3, 2010.

This research was supported by National Institute of Child and Health Development Grant HD2080. We are grateful to Jos Eggermont, Dan Tollin, and John Middlebrooks for helpful comments on a previous version of this manuscript. We thank Chen Chen and Francisco Rodriguez for related discussion and assistance with sound calibration. We are very grateful for the excellent and insightful input we obtained from the two anonymous reviewers.

Correspondence should be addressed to Heather L. Read at the above address. E-mail: heather.read@uconn.edu.

DOI:10.1523/JNEUROSCI.2561-10.2010

 0270-6474/10/3014522-11$15.00/0

fields. Distinct response distributions suggest ventral auditory cortices have specialized representation of binaural ILD cues.

Materials and Methods

Animals and surgery. Animals were housed and handled according to approved guidelines by the Institutional Animal Care and Use Committee at the University of Connecticut (Storrs, CT). Fourteen adult male rats (4 Wistar, 10 Brown Norwegian) were used in this study (age, 56–98 d; mean, 72 ±16 d; mean weight, 265 ± 65 g; obtained from Charles River Laboratories). No statistical differences were observed in BF, characteristic frequency (CF), or best ILD between albino and brown rats, so all animals were pooled into one group. Anesthesia was induced with sodium pentobarbital (<40 mg/kg, i.p.) for surgical procedures and supplemented as needed (20–50 mg/kg, i.p.) to maintain areflexia. Tracheotomy and cisterna magnum puncture were performed, and atropine sulfate (0.1 mg/kg) and dexamethasone (0.25 mg/kg) were administered to minimize respiratory noise and cerebral edema. Skull and dura were removed to expose temporal cortex in the right cerebral hemisphere. The exposure was covered with agar and sealed with a glass coverslip for optical imaging of intrinsic metabolic responses.

Sound delivery and design. Sounds were delivered diotically (same sound to both ears), dichotically (different sound levels to both ears), and monaurally (sound to one ear, other ear plugged). Sound stimuli were generated off-line with custom C++ or Matlab software (Mathworks) at a rate of 192 kHz and 24-bit resolution. Sounds were presented via hollow ear bars and calibrated for frequency distortions between 1 and 47 kHz (±3 dB) in the closed system with a 400-sample FIR inverse filter implemented on a RX6 multifunction processor [Tucker Davis Technologies (TDT)]. Speakers were tested and calibrated to assure linearity (input–output coherence >0.95) and matched transfer functions across custom modified (Beyer DT 770) speakers. Unit sounds were delivered with an RME DIGI 9652 or a TDT RX6 multifunction processor at 96 kHz. Optical sounds were delivered with a professional audio card (Lynx Studio Technology) at 98 kHz.

Sound stimuli. We found that the first spectral-notch attributable to the pinna and the pinna-dependent ILDs was most prominent for sound frequencies between 12 and 24 kHz in the rat (Koka et al., 2008); hence, tone frequency response sensitivities were probed between 2 and 32 kHz as described in detail previously (Polley et al., 2007; Higgins et al., 2008). The sound used to optically image BF organization consisted of 16 short-duration (5 ms rise time, 50 ms duration) tone pips separated by 250 ms intertone intervals to create ascending (2–32 kHz) or descending (32 to 2 kHz) tone staircase sequences with tones separated by one-fourth octave frequency steps. The sound used to estimate unit BF and its topographic organization contained 369 tone pips (5 ms rise time, 50 ms duration) varied randomly in one-eighth octave frequency steps from 1.4 to 44 kHz (500 ms intertone interval) and 10 dB sound level steps from 5 to 85 dB presented diotically over six trials.

ILD cue sensitivity can change with sound frequency content (Spezio and Takahashi, 2003) and average binaural level (ABL) (Tsai et al., 2010), therefore we used broad-spectrum noise to probe ILD over a range of ABLs, as a variation on the approach developed by Kitzes and colleagues (Semple and Kitzes, 1993a; Zhang et al., 2004). An "SPL × SPL stimulus matrix" probed sound pressure level (SPL), ILD, and ABL sensitivities and consisted of independent flat spectrum maximum length sequence noise tokens (<5 ms rise time, 50 ms duration, 2 Hz presentation rate) with SPL varied randomly in 5 dB steps ranging from 0 to 75 dB SPL for a total of 256 unique sound level combinations, and each condition in the matrix was presented 16 times.

Fourier optical imaging. A Fourier method of intrinsic optical imaging was used to map tone frequency responses in 14 animals across five cortical regions including A1, anterior auditory field (AAF), posterior auditory field (PAF), ventral auditory field (VAF), and suprarhinal auditory field (SRAF) as described previously (Kalatsky et al., 2005; Polley et al., 2007; Higgins et al., 2008). The Fourier method extracts intrinsic phase and magnitude responses to continuous (periodic) sound input resulting in a high spatial resolution image or map of cortical sound response properties. The camera was focused on the cortical surface while illuminating with green wavelength (547 ± 10 nm) filtered light to obtain a 4.6 × 4.6 mm^2 image of surface blood vessels. Next, the focus was translated down 650 μm (with a high-precision axial manipulator), and the reflectance of red (605 ± 10 nm) filtered light was recorded. Ascending and descending optical imaging tone sequences yielded similar frequency topography; therefore, hemodynamic delay was corrected by subtracting ascending and descending frequency maps to generate a frequency difference map as described previously (Kalatsky et al., 2003). The average frequency within a 50 × 50 μm area centered at the unit recording tract site was used to estimate optical BF at the same site where unit responses were subsequently recorded. High correlations were observed in the present study between unit and optical estimates of BFs for matched cortical position and sound level condition, as reported previously (Kalatsky et al., 2005; Mrsic-Flogel et al., 2006; Higgins et al., 2008).

Computing optical frequency gradients. Neighboring visual cortical areas have reversed topographic representations of the retina that can be quantified by computing the local response gradients (Sereno et al., 1994). This approach was taken here to quantify the direction and change of BF gradients at regional borders. The optical BF map was Gaussian filtered (SD, 162 μm) at each pixel before computing the local BF gradient. Maxima and minima in the Laplacian were used to locate mirror reversals in the BF gradient. Reversals in the BF gradient direction were observed at the borders between neighboring cortical areas including (1) PAF and A1/VAF, (2) A1 and AAF, (3) VAF and caudal SRAF, and (4) rostral SRAF and ventral AAF, as qualitatively assessed previously (Kalatsky et al., 2005; Polley et al., 2007). The nomenclature used here follows that described previously by Polley et al. (2007). A line (x-axis) was drawn between caudal and rostral local minima of the Laplacian maps. In all maps examined, this line bisected A1 and VAF into two equal cortical areas following previous conventions (Higgins et al. 2008). The perpendicular line (y-axis) was centered on the Laplacian minima located in ventral temporal cortex in the region previously defined as SRAF. This x–y coordinate system was used to divide the cortical areas into 45° radial sectors. The resulting regional sectors corresponded well with regional boundaries determined with visual inspection previously. Local BF gradient vectors within each radial sector were averaged to estimate the corresponding regional BF gradient. Average regional vectors were all rotated to align the A1/VAF–AAF bisecting line to 0° from the horizontal dimension for analysis.

Estimating unit frequency sensitivity. After acquisition of imaging data, the agar-glass window was removed, and insulated low-impedance (1–2 MΩ) tungsten electrodes were positioned in cortex at a depth corresponding to layer IV (550–650 μm). Responses to pure tones were measured from extracellular multiunit responses in A1, VAF, and SRAF. Variations in tone frequency and level were used to generate a frequency response area (FRA). Custom automated algorithms in MATLAB were used to estimate the statistically significant threshold and responses within the FRA (Escabi et al., 2007). The centroid frequency ($\overline{X}_m$) for the spike rate response distribution determined the BF at each sound level. CF was determined from automated routines, as the BF 10 dB above response threshold:

$$\overline{X}_m = \frac{\sum_k f \cdot \overline{\mathrm{FRA}}(X_k, \mathrm{SPL}_m)}{\sum_k \overline{\mathrm{FRA}}(X_k, \mathrm{SPL}_m)}$$

where $\overline{\mathrm{FRA}}$ is the statistically significant FRA ($\alpha = 0.05$), $X_k = \log_2(f_k/f_r)$ is an octave measure of frequency, f_r is the reference frequency, and SPL_m is the sound pressure level.

Computing ILD, ABL, and defining analysis window of response areas. Rate responses to the SPL × SPL stimulus matrix were used to create 16 × 16 SPL × SPL response areas. ILD and ABL were computed as the difference and average of SPL between contralateral and ipsilateral ears, respectively. These computed values were used to replot spike rate data as a function of ILD and ABL in the ILD × ABL response area.

Several steps were taken to limit the stimulus conditions and time windows used for analysis of the response area as described in detail previously (Escabi et al., 2007). Briefly, a significant onset response time window was determined from the poststimulus time histogram (PSTH)

elicited with all stimulus conditions in the SPL × SPL response area. The spontaneous spike rate was calculated from activity 50 ms before stimulus onset, and a significance threshold ($\alpha = 0.05$) was determined by assuming the spontaneous spiking activity follows a Poisson process. The onset time was defined as the first PSTH time point that exceeded the significance level, and the offset was defined as the first time point after the onset time where the response was no longer significant. Thus, the SPL × SPL responses were calculated individually for each multiunit site by measuring the mean firing rate within the response window. There was no significant onset-duration window difference observed between regions (one-way ANOVA: $F_{(3,411)} = 0.72$; $p = 0.54$). A1, VAF, caudal SRAF, and rostral SRAF had median onset response durations of 29.5, 30.4, 32.1, and 28.4 ms, respectively. Collicular and PAF spatial receptive field centers remain constant when probed with noise levels between 10 and 40 or 20 and 40 dB above threshold (Middlebrooks and Knudsen, 1984; Stecker et al., 2005b). Likewise, preliminary analysis in the present study found best ILDs remained constant when the ILD × ABL response area window was limited from threshold to 40 dB above threshold. Hence, the ILD × ABL response area analysis window included the physiologic ILD range (±40 dB) characterized previously (Koka et al., 2008) and an ABL range from threshold to 40 dB above ABL threshold.

Data were also analyzed with a 10 dB analysis window of ±5 dB around maximal ABL and ILD response for each site. The spike rate curves for a 10 versus 40 dB window were highly correlated and had median similarity indices of 0.88 and 0.6 for ILD and ABL, respectively. Here we report results using the 40 dB analysis window.

Estimating best ILD and best ABL. Maximal or "best" ILD responses have been used to correctly predict the horizontal position preference of cells with BFs above 2 kHz (Fuzessery et al., 1990; Clarey et al., 1994). A similar approach was used here to estimate best ILD and best ABL. Spike rate in the analysis window for the ILD × ABL response area was collapsed in ILD and ABL dimensions to analyze corresponding rate-level responses. Rate level responses were fit with three response models including linear and Gaussian functions and a five-parameter sigmoid function of the following form:

$$y = \frac{a}{1 - e^{(-b \times (x - c))}} \cdot \left[1 - \frac{1}{1 - e^{(-d \times (x - e))}}\right]$$

where x is ILD, y is the discharge rate, and a, b, c, d, and e are free parameters. The five-parameter sigmoid function essentially fits the rising and falling (ipsilateral and contralateral) components of the rate ILD function with corresponding sigmoid functions and was motivated by evidence that the rate ILD function in lateral superior olive can be predicted based on a similar model (Tsai et al. 2010). The parameters b and d account for the rising and falling slopes of the ILD functions, whereas c and e correspond to the inflection points of the rising and falling sigmoid components. The variable, a, is a scaling factor to account for the peak response amplitude.

For each of the models, 8 of the 16 response trials were selected for model optimization, and the model parameters were obtained using the least squares procedure. The remaining eight trials were used for model validation to determine the amount of response variance explained by the model. The model fit and validation were bootstrapped 500 times to derive error bounds on the model parameters and the prediction quality. Using 1000 bootstrapped variations on a subset of the data yielded similar results. For each model, the prediction quality was determined by computing the correlation coefficient between the model and validation data (R_{linear}, R_{Gaussian}, R_{sigmoid}). Using the bootstrapped R values, we performed a three-way rank-sum test to determine which model best predicted the data. The model (linear, Gaussian, or sigmoid) that best accounted for the variance across bootstrapped iterations (highest median R value) was considered the best fit. Unit best ILD was defined as the average level evoking the maximal spike rate for each iteration of the best-fit model.

Computing binaural interactions. Binaural response interactions not only create aural dominance (i.e., aural response bias) properties, they also determine the tuning of SPL × SPL response areas (and therefore ILD × ABL response areas (Semple and Kitzes, 1993b). To quantify binaural interactions, we computed a binaural interaction index (BII) as the percentage of binaural response relative to the summed monaural responses for matched SPL:

$$\text{BII} = \frac{R(\text{SPL}_c, \text{SPL}_i)}{\text{R}(\text{SPL}_c) + R(\text{SPL}_i)} \times 100$$

where SPL_c and SPL_i are the contralateral and ipsilateral SPLs, $R(\text{SPL}_c, \text{SPL}_i)$ is the response rate to a binaural configuration, and $R(\text{SPL}_c)$ and $R(\text{SPL}_i)$ are the response rates for contralateral and ipsilateral stimulation, respectively. Since the analysis only considers responses that are above spontaneous levels, this method of computing BII resembles closely that used previously by Goldberg and Brown (1969). BII values >100 are facilitated, and values <100 are suppressed relative to the monaural inputs at the same level. The BII matrix was derived directly from the SPL × SPL matrix, therefore the spike-timing window and significance criteria apply to both the spike rate and BII plots. Mean BII collapsed across ABL dimension was plotted as a function of each ILD condition to generate population binaural facilitation curves. Data were analyzed from two datasets: (1) using the entire ±40 dB ILD–ABL range outlined above and (2) the same ILD–ABL range but excluding ipsilateral/contralateral SPL combinations that fell below contralateral threshold. Contralateral threshold was based on statistical comparison with spontaneous rate as described above and required more than one consecutive significant level. Subcontralateral threshold responses were linearly shifted in Figure 2*C* and excluded from all statistics and analysis presented except the population BII data in Figure 8, *A1* and *B1*.

Estimates of receptive field tuning. In superior colliculus of the cat, spatial receptive field widths vary as a function of spatial receptive field centers estimated from 75% of the maximum spike rate response (Middlebrooks and Knudsen, 1984). Here we queried whether a similar relationship existed between ILD tuning width and best ILD. All units examined here responded to a restricted range of negative ILDs, corresponding to ipsilateral sound position cues. Thus, we were able to quantify the ipsilateral ILD tuning width of the rate ILD response curve. Ipsilateral "half-width" was estimated as the difference between best ILD and ILD corresponding to 75% of the maximum response on the ipsilateral side of the function. Some cortical units (e.g., hemifield units) respond to all the contralateral ILD cues in the test area and therefore have a width equal to or greater than the tested range of ILDs greater than zero. For the latter units, it is not possible to compute the tuning width for ILDs above the best ILD. To overcome this limitation and to allow for comparisons across units with varying degrees of tuning to contralateral ILD cues, the degree of tuning to contralateral ILD cues was measured by calculating the percentage drop in spike rate after the maximum, a measure typically used to quantify rate-level curve monotonicity (Nakamoto et al., 2004). Both measures of tuning were calculated for each iteration of the bootstrapped best-fit model, and the average of these values for each unit was used for further analysis.

Statistical analysis. Results are based on multiunit responses to ILD noise in A1 ($n = 159$), VAF ($n = 94$), caudal SRAF ($n = 91$), and rostral SRAF ($n = 71$). Of the total 415 responses, 336 contributed FRAs to the dataset. A Lilliefors' composite goodness-of-fit test for normality was applied to all distributions before statistical comparison. Unless noted otherwise, all statistical comparisons were done using the Wilcoxon rank-sum test for equal medians because of the not normal nature of the dataset.

Results

Sound reflections off the rat's pinnae create frequency cues that change linearly with vertical position of sound over ±60° in the frontal sound field (Koka et al., 2008). BF has been used in subcortical structures as a metric of neural sensitivity to pinna-related frequency cues (Davis and Young, 2000; Chase and Young, 2005). Here we used high-resolution intrinsic optical imaging to map cortical sensitivity to tone frequency and BF (Kalatsky and Stryker, 2003; Kalatsky et al., 2005). Six cortical fields each contained a separate representation of sound fre-

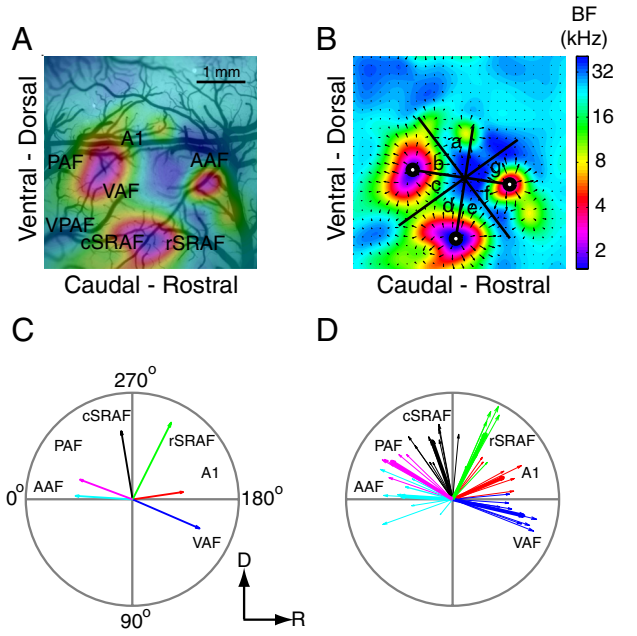

Figure 1. High-resolution optical imaging used to determine regional borders of auditory cortex. ***A***, Surface blood vessel image overlaid with map of optical BF obtained at 650 μm below the surface with an ABL of 45 dB (SPL). Three local minima in BF (<2 kHz) are observed in temporal areas 1 (Te2), 2 (Te1), and 3 (Te3). ***B***, Gradient direction for change in BF was determined by computing the BF gradient. The corresponding local frequency vector map is overlaid with the BF map to illustrate the local gradient directions for change in BF. White circles indicate the BF and Laplacian minima in Te1–Te3 used to divide the cortex into radial sectors a–g (see Materials and Methods). Sectors were assigned to cortical fields defined physiologically and anatomically previously (Kalatsky et al. 2005; Polley et al. 2007). Primary auditory cortex (A1) includes sectors a and b. VAF and caudal (cSRAF) and rostral suprarhinal (rSRAF) auditory fields correspond to sectors c–e, respectively, and AAF corresponds to sectors f and g. ***C***, Local vectors were averaged in each cortical field to obtain the regional vector average. Data shown are for the frequency map given in ***A***. ***D***, Regional average vectors for maps obtained in nine rats. Thick lines indicate mean of population. D, Dorsal; R, rostral; VPAF, ventral posterior auditory field.

quency (2–32 kHz), and the range of BFs mapped in all regions covered the range of pinna-related frequency and ILD cues in the rat (Koka et al., 2008; Tollin and Koka, 2009). A1, VAF, SRAF, and AAF had optically measured tone frequency responses with topographic or "cochleotopic" BF organization like that of the cochlear epithelium of the ear (Kalatsky et al., 2005). Here optically measured response cochleotopy was also observed in PAF of six animals (Fig. 1*A*). We computed the local BF gradient to quantify the direction of frequency change and overlaid the computed direction vectors to illustrate the local gradients (Fig. 1). The Laplacian of the BF gradient map was used to locate reversals in BF gradient direction. BF and Laplacian minima and maxima of the corresponding maps were used to divide cortical regions into radial sectors (Fig. 1*B*, sectors a–g). Each cortical region was characterized by a distinct summed BF gradient vector orientation as shown for the right cerebral hemisphere from one animal (Fig. 1*C*). PAF and A1 shared a common BF minimum and had reversed BF gradient directions, as predicted from unit response maps (Doron et al., 2002; Pandya et al., 2008). BF gradients reversed at the border between VAF and caudal SRAF and between A1 and AAF resulting in opposing summed vector directions. Similar BF gradient vector orientations were observed in PAF of six animals, and all other regions were examined in nine animals (Fig. 1*D*). Therefore, frequency sensitivity and BF gradient orientation were considered stable organizational features and used to delineate regional borders. The frequency distributions from each region were not significantly different from each other (one-way ANOVA comparing CF in each region; $F_{(3,330)} = 1.12$; $p = 0.3417$), ensuring regional differences in response parameters were not the result of unequal sampling.

A1 responds with a full and continuous range of neural sensitivities to horizontal position cues in the contralateral sound hemifield (Semple and Kitzes, 1993b; Zhang et al., 2004; Campbell et al., 2006b) as does PAF in the cat (Harrington et al. 2008). However, current models imply that ventral auditory cortices do not respond to spatial cues with any specificity (for review, see Romanski, 2004). Here we revisit this question of spatial cue sensitivity by directly comparing spatial response properties in A1 and ventral auditory cortices. Responses to ILD horizontal position cues were probed with broad-spectrum noise (see Materials and Methods) within the physiological range determined from the measurements of acoustic directional transfer functions (Koka et al., 2008). Multiunit response areas were plotted as a function of ipsilateral (right) and contralateral (left) ear sound level (Fig. 2*A1–A5*). Response areas were also plotted as a function of the corresponding computed ABL and ILD (Fig. 2*B1–B5*). The example A1 unit had high spike rates over a broad range of positive ILDs, indicating a broad sensitivity to sound positions in the contralateral hemifield, as was typical of A1 responses (Fig. 2*B1*, red voxels). The example VAF and caudal SRAF units illustrate high spike rate over a restricted range of ILD and ABL, as was typical of these two regions (Fig. 2*B2*,*B3*, red voxels). The example rostral SRAF units spiked maximally (red voxels) with high ABL, as was typical of this region (Fig. 2*B4*,*B5*). In general, these units exemplify the more narrow range of ILD sensitivities in VAF and caudal SRAF response areas (Fig. 2).

For a subset of A1 neurons, response tuning to horizontal position cues is shaped by facilitative and suppressive interactions across auditory pathways for the left and right ear (Semple and Kitzes, 1993b; Spezio and Takahashi, 2003; Zhang et al., 2004; Popescu and Polley, 2010). However, for the majority of A1 neurons, spatial receptive field properties can be predicted without accounting for these binaural interactions, suggesting they play a relatively minor role in shaping A1 response areas (Schnupp et al., 2001; Mrsic-Flogel et al., 2005). Here we questioned whether binaural interactions could account for the narrower ILD response areas observed in VAF and SRAF. Our approach assumed no binaural interaction occurred if binaural sound conditions eliciting spike rates were equal to the summed spike rate elicited with each ear alone. If spike rate with the binaural condition was >100% or <100%, we assumed there was binaural spike rate facilitation or suppression, respectively. The example A1 and VAF units both had about 20% binaural facilitation (BII, 120%; cyan voxels) for binaural sound levels near the condition corresponding to best ABL and best ILD (open circle) for each unit (Fig. 2*C1*,*C2*). Binaural suppression (BII, 60%; blue voxels) was evident with ipsilateral ILD position cues for the examples from A1, VAF, and caudal SRAF (Fig. 2*C1–C3*). The example caudal SRAF site had maximal spike rate (Fig. 2*B3*) and high binaural facilitation (Fig. 2*C3*) for ILD position cues near midline (ILD, 0), as was characteristic of this field. All three SRAF units had robust binaural facilitation at sound levels below and above threshold for spike rate response to contralateral ear (Fig. 2*C3–C5*, red-brown voxels above and below white dashed line). These examples demonstrate that unit responses can be shaped by binaural interactions in all cortical fields.

Although A1 cortical neurons are relatively selective to frequency content of sound, they generally have broadly tuned responses to ABL and horizontal position cues (Eggermont, 2001;

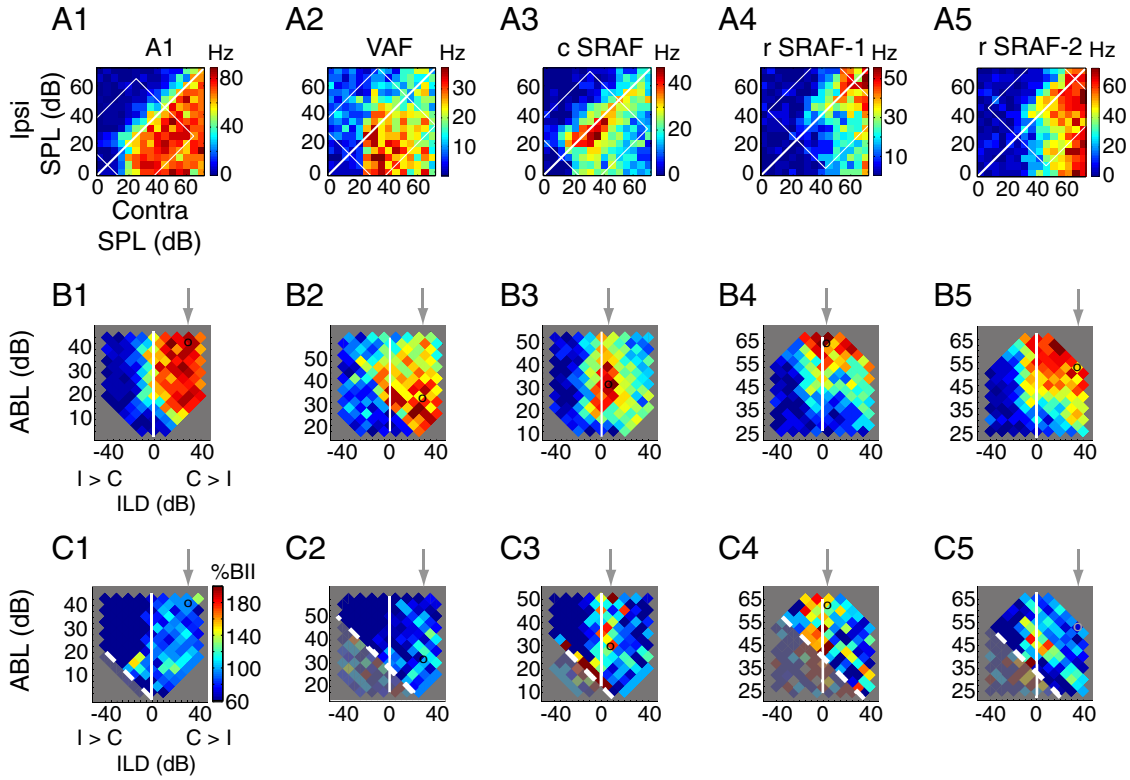

Figure 2. Examples of commonly observed response areas and binaural interaction areas for each cortical field. ***A1–A5***, SPL was varied from 0 to 75 dB in each ear to test monaural and binaural sound level conditions and generate "SPL response areas." The color spectrum indicates spike rate per second (in hertz) elicited with each condition. The white diagonal line indicates midline condition (ILD, 0). The white box outlines the ILD (ILD, ±40 dB) and ABL (ABL = threshold + 40 dB) ranges used to generate ILD × ABL response areas in ***B***. Ipsi, Ipsilateral; Contra, contralateral. ***B1–B5***, ILD × ABL response areas corresponding to the white box in ***A***. White line, Color spectra are the same as in ***A***. Arrows represent best ILD. Positive *x*-axis values represent conditions where the contralateral (C) level was louder than the ipsilateral (I) level. The black circle represents the intersection of best ILD and best ABL computed as shown in Figure 3. ***C1–C5***, Binaural interaction areas derived from example responses shown in ***A*** and ***B***. The color spectrum indicates BII where values below and above 100% are suppressed and facilitated, respectively, relative to the sum of monaural responses at the corresponding SPL. The thin solid white line and thick dashed white line indicate midline and contralateral response threshold, respectively. cSRAF, Caudal suprarhinal auditory field; rSRAF, rostral suprarhinal auditory field.

Schnupp et al., 2001; Stecker et al., 2005b; Campbell et al., 2006b; Popescu and Polley, 2010). Here we queried whether similar trends are observed in ventral cortices outside of A1. To quantify the ABL and ILD tuning at each recording site, corresponding rate-level curves were fit to linear, Gaussian, and sigmoid functions (see Materials and Methods). For representative A1 and VAF units, the spike rate increased with ILD, and best ILDs (open circles) were >30 dB (Fig. 3*A1*,*A2*). For the VAF unit, the spike rate dropped by a small percent when ILD was higher than best ILD (Fig. 3*A2*). The example A1 and VAF sites had broad monotonic and narrow nonmonotonically tuned responses to ABL, respectively (Fig. 3*B1*,*B2*), confirming reports of distinct ABL sensitivities for these two regions (Polley et al., 2007; Higgins et al., 2008). The example caudal SRAF response was nonmonotonically tuned in ILD and ABL dimensions that were best fit with the double sigmoid and Gaussian functions, respectively (Fig. 3*A3*,*B3*). The first example rostral SRAF unit response was tuned in ILD but not ABL (Fig. 3*A4*,*B4*), and the second was monotonically saturated with a high level in both dimensions (Fig. 3*A5*,*B5*). These five examples confirm previous reports of coarse tuning in A1 and demonstrate relatively narrow tuning to ABL and horizontal spatial cues in two additional ventral cortical regions.

Monaural and binaural responses and corresponding binaural interactions in rat auditory cortex were similar in many respects to those described previously in other mammals. Historically, the standard classification scheme used to characterize monaural and binaural response types was developed to describe subcortical neurons of the dog. This scheme labels spike rate response as excitatory (E), inhibitory (I), or null (O) for contralateral and ipsilateral ear in the first two consecutive fields and binaural interaction type as facilitative, suppressive, or null (occlusion) in the third field (Goldberg and Brown, 1969; Zhang et al., 2004). Four example ILD response areas from the present study were categorized according to such a scheme in Figure 4. The first example unit, was less excited by high binaural sound levels (SPL, >20; cyan/blue pixels) than by low monaural contralateral or ipsilateral sound levels (SPL, 20; red voxels) and would be classified as an EE/S type, where S indicates a suppressive binaural interaction for ipsilateral ILD cues (Fig. 4*A1*,*A2*). The second unit had E and O responses to monaural sound in the contralateral and ipsilateral ears, respectively (Fig. 4*B1*,*B2*). This unit was binaurally suppressed (S) when sound was louder in the ipsilateral ear; hence, it would be an EO/S according to this scheme (Zhang et al., 2004); however, this response type also has been called EI (Goldberg and Brown, 1969; Middlebrooks et al., 1980). According to this scheme, a true monaural response would have excitation with one monaural condition, null with the other, and no binaural interaction (EO/O type). In the present study, many responses came close to fitting the monaural profile (Fig. 4*C*), but all generally had some degree of binaural suppression for ipsilateral ILDs, making them EO/S. Exemplar responses illustrate how cells in SRAF were alternately suppressed, facilitated, and suppressed by ipsilateral, midline, and contralateral ILDs,

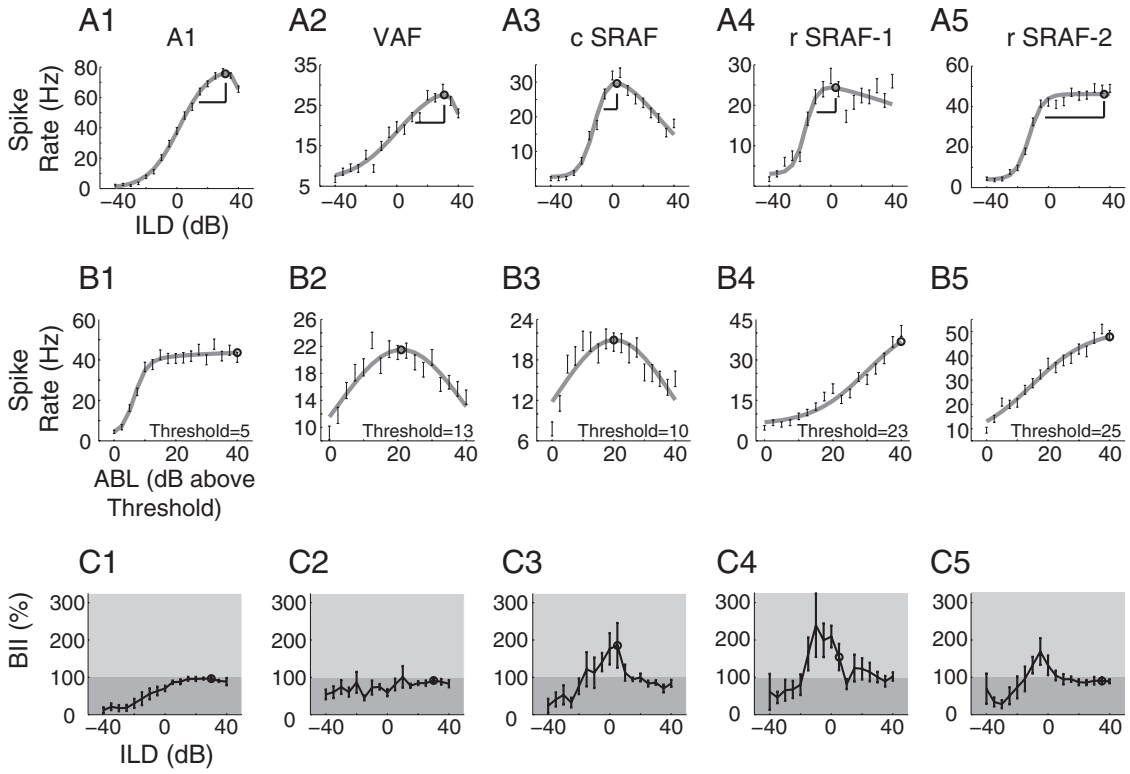

Figure 3. Fits of rate-level functions and corresponding binaural index curves. ***A1–A5***, Mean ILD spike rate (SEM error bars) and significant best fits (gray function) for same cortical site examples shown in Figure 2. The preferred horizontal position was estimated as the maximum of the rate ILD function or best ILD (black circle). Half-width at 75% of the maximum spike rate was a metric of response tuning for ILDs ipsilateral to best ILD (black perpendicular lines indicate intersections used to compute half-width). ***B1–B5***, Mean ABL spike rate and significant fits (same conventions as in ***A***). Black circles indicate best ABL. ***C1–C5***, Curves from corresponding BII response areas shown in Figure 2. The black circle indicates best ILD computed from functions shown in ***A***, Light and dark shading represents binaural facilitation and suppression, respectively. cSRAF, Caudal suprarhinal auditory field; rSRAF, rostral suprarhinal auditory field.

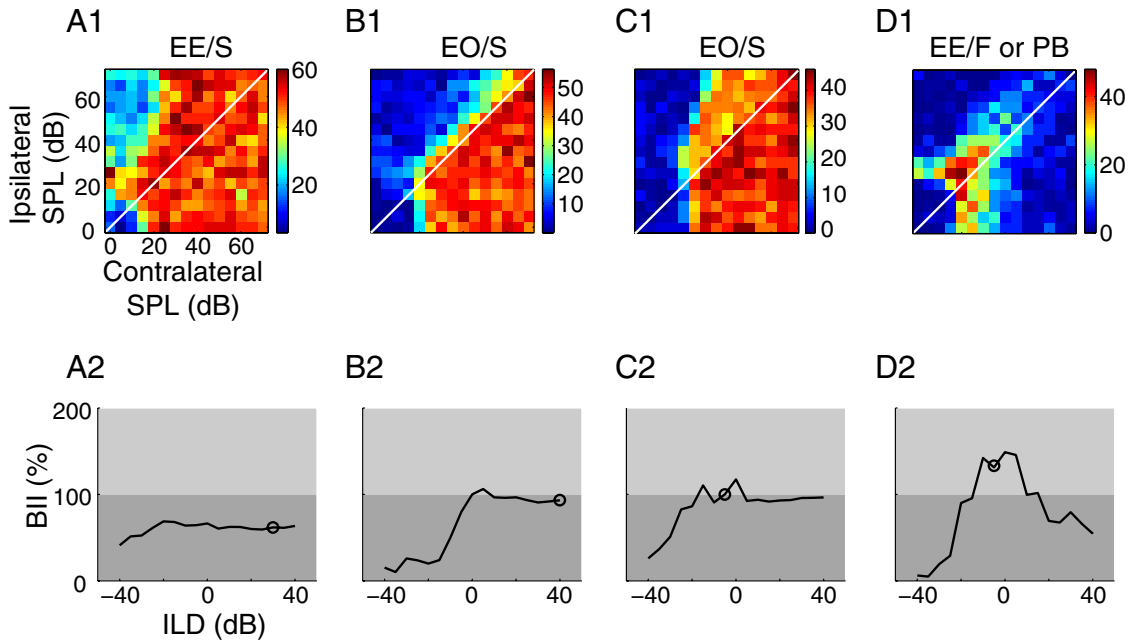

Figure 4. Examples of traditional binaural response profiles observed in rat auditory cortex. ***A***, EE/S unit is monaurally excited at low sound levels and displays no increased response to binaural. BII is very low because of high monaural response relative to binaural combinations. ***B***, EO/S unit is excited by contralateral stimulation and has a null response to ipsilateral stimulus with suppressed binaural interaction observed in the BII–ILD curve. ***C***, EO/O (S) unit excited by contralateral stimulation and with moderately suppressed BII for ipsilateral ILDs. ***D***, EE/F or predominantly binaural (PB) unit responds preferentially to matched contralateral–ipsilateral SPL combinations. The BII–ILD curve is characterized by significant facilitation around the midline and significant ipsilateral and contralateral suppression. Error bars are removed for illustrative purposes.

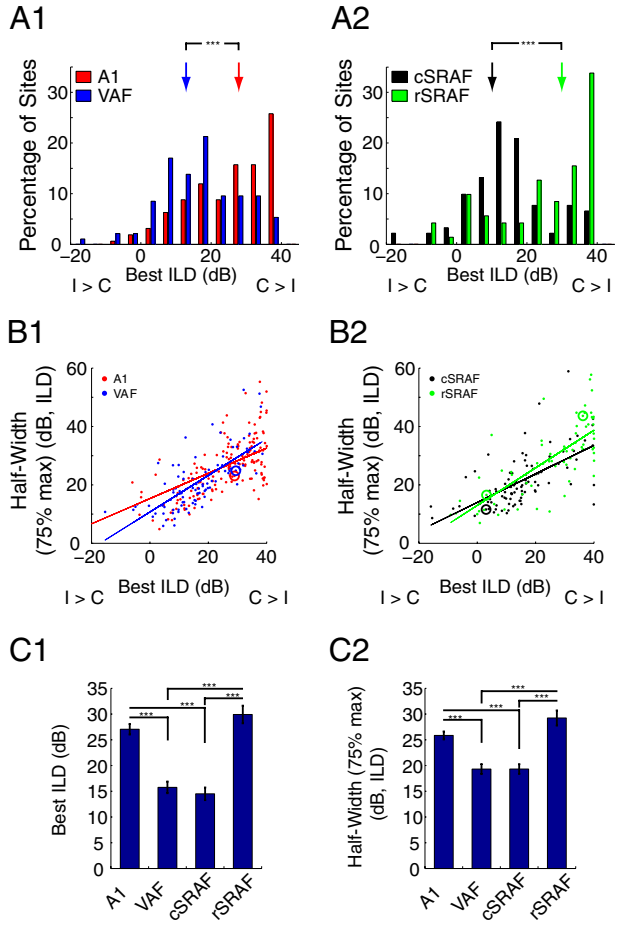

Figure 5. Best ILD and ipsilateral half-widths were smallest in VAF and cSRAF. ***A1***, ***A2***, Continuous distributions of estimated best ILDs for units from each cortical field. Arrows indicate the median (***$p < 0.001$). ***B1***, ***B2***, Best ILD correlates significantly with the half-width in all regions ($p < 0.001$). Circles indicate example units in Figure 2. ***C1***, ***C2***, Bars represent the median and SEM (***$p < 0.001$) I, Ipsilateral; C, contralateral; max, maximum; cSRAF, caudal suprarhinal auditory field; rSRAF, rostral suprarhinal auditory field.

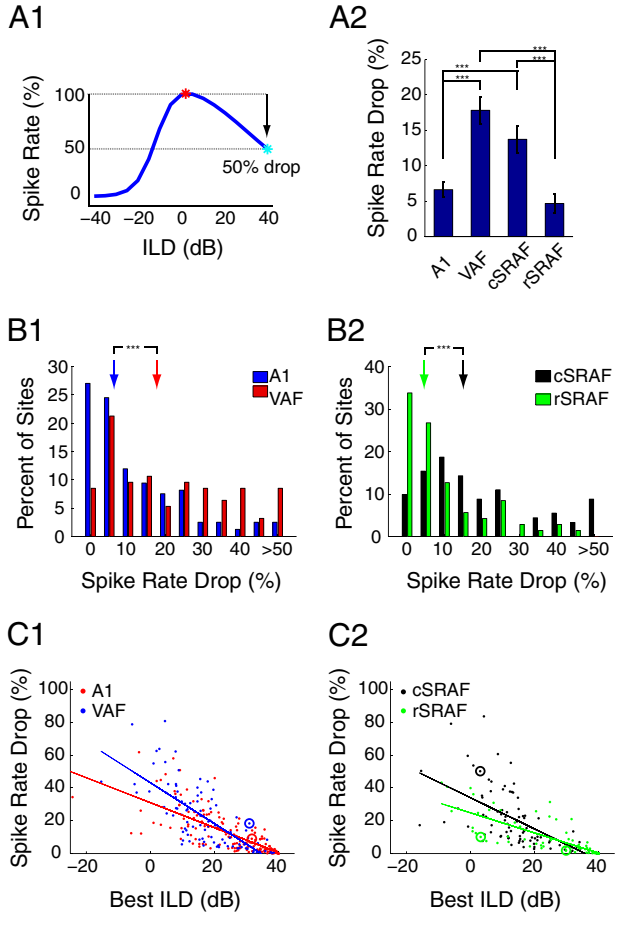

Figure 6. Spike rate reductions with contralateral ILDs were largest in VAF and cSRAF. The percentage drop from the peak of spike rate function was computed as a metric of response tuning for ILDs contralateral to best ILD. ***A1***, Example rate-level function illustrating a 50% drop in spike rate after the peak. ***A2***, Median spike rate drop in each region (***$p < 0.001$). ***B1***, ***B2***, Continuous distributions of contralateral spike rate drop for units from each cortical field. Arrows indicate the median. ***C1***, ***C2***, Best ILD correlates significantly ($p < 0.001$) with spike rate reduction after peak in all regions. Circles indicate example units in Figure 2. cSRAF, Caudal suprarhinal auditory field; rSRAF, rostral suprarhinal auditory field.

respectively (Figs. 2*C3*, 4*D*). According to the classic scheme, these would be EE/F-type responses, and according to other schemes, these would be "primarily binaural" or "two-way-intensity" tuned (Semple and Kitzes, 1993b; Pollak et al., 2002; Zhang et al., 2004; Razak and Fuzessery, 2010). These historically useful categorization schemes do not adequately categorize variation in binaural interactions as a function of ipsilateral versus contralateral ILD conditions prevalent in cortical regions outside of A1.

Subcortically, horizontal spatial receptive field size increases with eccentricity of maximal response or receptive field center (Middlebrooks and Knudsen, 1984; Rowland et al., 2007). To examine this relationship in cortex, we computed best ILD and ILD half-width from the significant fits of corresponding rate-level curves (Fig. 3*A*). The distributions of best ILDs were overlapping but significantly different for neighboring cortical fields (Fig. 5*A1*,*A2*) (rank-sum test, $p < 0.001$). For all cortical regions examined, half-widths were continuously and positively correlated to best ILD (Fig. 5*B1*,*B2*) (A1, $r = 0.58$; VAF, $r = 0.73$; caudal SRAF, $r = 0.63$; rostral SRAF, $r = 0.75$; $p < 0.001$ for all regions). The median best ILD was smaller in VAF and caudal SRAF than in A1 and rostral SRAF (one-way ANOVA; $F_{(3,411)} = 17.15$; $p < 0.001$, *post hoc* rank-sum, $p < 0.001$), indicating a bias for midline best ILDs in VAF and caudal SRAF (Fig. 5*C1*). Likewise, the median half-width was smaller in VAF and caudal SRAF than A1 and rostral SRAF (one-way ANOVA; $F_{(3,411)} = 12.19$; $p < 0.001$, *post hoc* rank-sum comparisons, $p < 0.001$), indicating narrow tuning to ipsilateral ILD cues (Fig. 5*C2*). Hence, cortical sites with best ILDs near zero had the smallest half-widths. This quantitative analysis found VAF and caudal SRAF were maximally sensitive to midline horizontal position cues and more narrowly tuned to ipsilateral ILD cues than their counterparts in A1 or rostral SRAF.

A metric for tuning to contralateral horizontal position cues is the percentage drop in spike rate for ILD greater than best ILD. An example rate ILD level curve, illustrates a 50% drop in spike rate for ILDs greater than the best ILD (Fig. 6*A1*). This drop in spike rate effectively tuned the response to a narrow range of contralateral horizontal position cues around the midline. Tuned responses like this were more common in VAF and caudal SRAF, and the corresponding median spike rate drop was greater for VAF and caudal SRAF than for A1 and rostral SRAF (Fig. 6*A2*) (one-way ANOVA; $F_{(3,411)} = 14.22$; $p < 0.001$, *post hoc* rank-sum comparisons, $p < 0.001$ for A1 vs VAF, A1 vs caudal SRAF, VAF vs rostral SRAF, caudal SRAF vs rostral SRAF). VAF and caudal

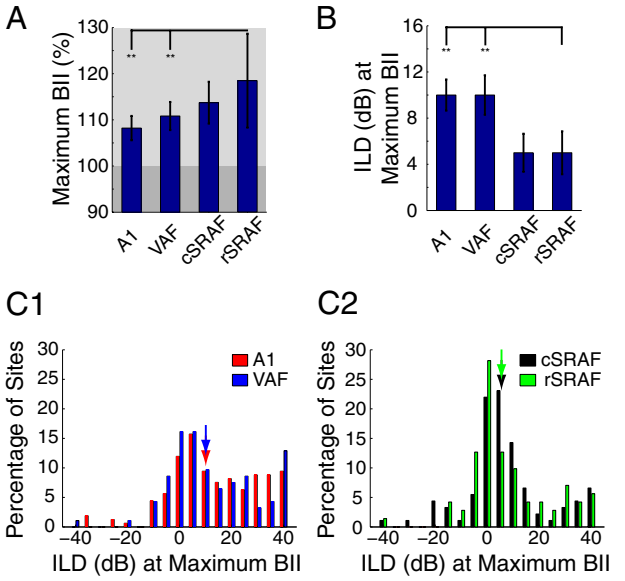

Figure 7. Percentage of binaural facilitation was largest for near-midline ILDs in rostral SRAF. ***A***, Regional differences in median BII (**$p < 0.01$). ***B***, Median ILD value corresponding to maximum BII (see Materials and Methods; **$p < 0.01$). Error bars represent SEM. ***C1***, ***C2***, Continuous distributions of ILDs at maximum BII for each cortical field. Arrows indicate the median. cSRAF, Caudal suprarhinal auditory field; rSRAF, rostral suprarhinal auditory field.

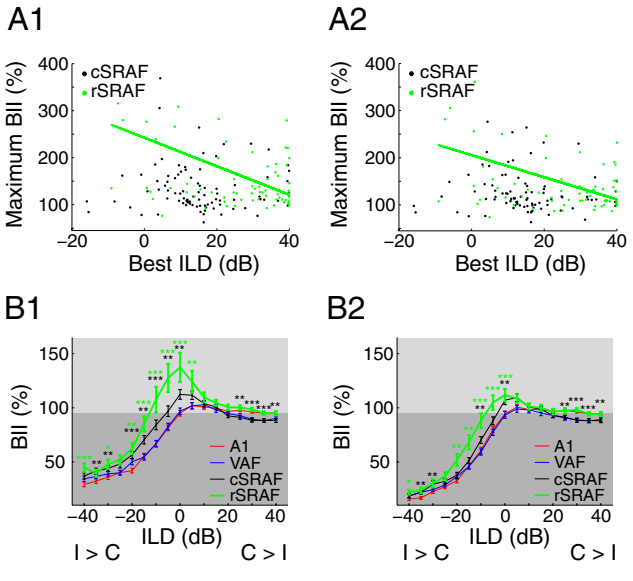

Figure 8. Binaural interactions highest for near-midline ILDs in caudal and rostral SRAF. ***A1***, ***A2***, Best ILD and maximum BII were above 100% in both caudal (cSRAF) and rostral (rSRAF) SRAF and were inversely related in rostral SRAF. The maximum BII was measured from unit BII curves generated with all sound levels in the ILD response area (***A1***) (see Fig. 3*C1–C5*) or with levels below contralateral ear threshold removed (***A2***). ***B1***, ***B2***, Population BII ILD curves illustrate the high-percent facilitation for near-midline ILDs in caudal and rostral SRAF and the lack of significant facilitation in A1 and VAF. Population BII curves averaged across ABL dimension of the BII response areas (***B1***) or with levels below contralateral ear threshold removed (***B2***). Light and dark shading indicates binaural facilitation and suppression, respectively. Error bars represent SEM (*$p < 0.025$; **$p < 0.01$; ***$p < 0.001$). I, Ipsilateral; C, contralateral.

SRAF had contralateral spike rate drops >20% in 47 and 38% of units, respectively, whereas A1 and rostral SRAF sites had drops of that magnitude in just 23 and 20% of units, respectively (Fig. 6*B1*,*B2*). For all cortical regions examined, the percentage drop in spike rate was continuously and inversely correlated to best ILD (Fig. 6*C1*,*C2*) (A1, $r = -0.76$; VAF, $r = -0.74$; caudal SRAF, $r = -0.62$; rostral SRAF, $r = -0.78$; $p < 0.001$ in all regions). Hence, cortical sites with best ILDs near zero had the largest percentage drop in rate indicating a more narrowly tuned response to contralateral hemifield cues.

The degree of binaural facilitation was highest in the ventral cortical field, SRAF. To compare binaural facilitation across cortical regions, the maximal facilitation and its corresponding ILD value were estimated for each site from the binaural interaction curve (Fig. 3*C1–C5*). Binaural facilitation was larger in rostral SRAF than any other region (Fig. 7*A*) [one-way ANOVA; $F_{(3,402)} = 6.53$; $p < 0.001$ across region, with *post hoc* rank-sum comparisons showing significant differences between A1 and VAF vs rostral SRAF ($p < 0.01$; Bonferroni correction; $\alpha = 0.0125$]. Maximum binaural interaction (i.e., facilitation) was highest for midline ILDs in SRAF (Fig. 7*B*,*C2*) (one-way ANOVA; $F_{(3,410)} = 4.64$; $p < 0.01$) and more distributed over a range of ILDs in A1 and VAF (Fig. 7*B*,*C1*). *Post hoc* comparison of individual regions shows rostral SRAF has significantly more midline facilitation than A1 and VAF (rank-sum comparisons, $\alpha = 0.0125$). Caudal SRAF also trended toward more midline facilitation than A1 and VAF but did not meet the adjusted α level. Binaural facilitation was observed (Fig. 3*C*) and inversely related to best ILD in A1, VAF (data not shown), and rostral SRAF; however, the slope of this relationship was greatest for rostral SRAF (Fig. 8*A1*). This relationship was similar for maximum BII that occurred throughout the response area (Fig. 8*A1*) ($r = -0.41$; $p < 0.001$) or for the limited area above response threshold for sound in the contralateral ear (Fig. 8*A2*) ($r = -0.40$; $p < 0.001$). Regional differences in binaural facilitation were also evident in the population curves (Fig. 8*B1*,*B2*) (mixed-design ANOVA; $F_{(1,3)} = 14.79$; $p < 0.001$ between regions) even when all samples below contralateral threshold are removed (Fig. 8*B2*) (repeated-measures ANOVA; $F_{(3,1)} = 10.02$; $p < 0.001$ between regions). SRAF but not A1 and VAF population curves had high-percent (BII, >120%) binaural facilitation at midline ILDs (ILD, <20 dB).

Discussion

This study addresses the question of whether ventral auditory cortices systematically represent or encode sound position cues. Binaural ILD sensitivities were measured as these are directly related to horizontal sound position sensitivity (Wenstrup et al., 1988; Campbell et al., 2006a,b). Best ILDs were highest in A1 and rostral SRAF, indicating sensitivity to more contralateral horizontal sound positions. The border between VAF and caudal SRAF was marked by a mirror reversal in BF gradient, yet both regions responded optimally to midline horizontal positions cues. This suggests that ILD sensitivities are organized into a meta-gradient distinct from the BF gradient (Polley et al., 2007). Response tuning to ILD was inversely related to best ILD, and the highest degrees of ILD tuning were observed in VAF and caudal SRAF. Although binaural facilitation was observed at individual sites throughout all regions examined, this response profile was most prevalent in caudal and rostral SRAF. We conclude that sound localization cues are a key organization feature in A1 and ventral auditory cortices, and the high degree of binaural facilitation in SRAF distinguishes this ventral region from neighboring VAF.

One of the interesting large-scale organizational features apparent from this study is that ILD tuning does not abide by the BF gradients that define each cortical field. BF tuning in caudal SRAF is similar to and contiguous with that of rostral SRAF, but its ILD

tuning is contiguous with and similar to VAF. This suggests that caudal SRAF and VAF form a "superfield" that does not abide conventionally defined cortical region boundaries such as mirror reversals in the BF gradient. This same regional organization with respect to ABL intensity cues was described in a previous paper as a meta-gradient (Polley et al., 2007). Studies that only characterize one field at a time fail to appreciate the existence of response properties that are spatially mapped as meta-gradients that can extend across conventional cochleotopic boundaries. Horizontal sound position sensitivity varies from midline to contralateral eccentricities in a topographic pattern that appears to extend across regional boundaries in ferret cortex [Bizley et al. (2009), their Fig. 3]. Thus, superfield and meta-gradient organization may be a universal property of auditory cortex organization in mammals.

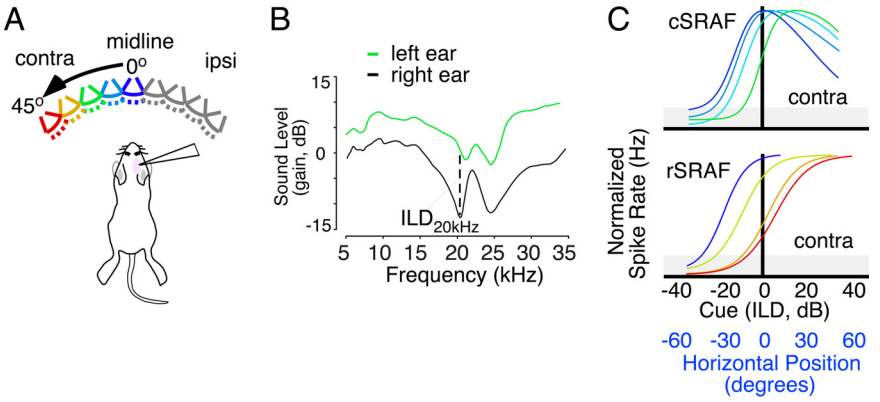

Figure 9. Recording, playing, and encoding binaural sound level horizontal position cues. ***A***, Spatial schematic for recording ILD cues and neural sensitivities to horizontal position change in cortex of right cerebral hemisphere. Speaker icons represent position steps in horizontal or azimuth dimension. ipsi, Ipsilateral; contra, contralateral. ***B***, Rat transfer functions recorded in left/right ears at one position (22.5° azimuth, 0° elevation). The largest right and left ear pinna-dependent reflections are centered near 20 and 25 kHz, respectively. The dotted line indicates ILD at 20 kHz. ***C***, Best fits of ILD versus spike rate response curves for a subset of sites in this study. Responses to noise ILD are narrow and broad in caudal (cSRAF) and rostral (rSRAF) SRAF, respectively. Horizontal positions estimates are based on previous studies (Koka et al., 2008).

Binaural ILD response sensitivities in A1 and ventral auditory cortices could create a spike rate code for directing attention toward auditory objects. Each time a mammal directs its gaze or head toward a sound in the scene, it creates a spatial framework relative to the body midline (Fig. 9*A*). Because of reflection of sound off the head and pinnae, sounds located to the left of the sensory field midline are louder in the left versus right ear (Fig. 9*B*, green vs black line). For a given sound position, ILD cues may be computed for one sound frequency (Fig. 9*B*, 20 kHz dotted line), but they exist over a range of sound frequencies as illustrated for exemplar transfer functions recorded from a rat when noise was played from a speaker positioned 22.5° to the left of midline (Fig. 9*B*). All ILD responses characterized here were fit with one of three functions (see Materials and Methods), and best ILD was estimated as the maximum of the significant fit. Near midline, best ILDs were most prevalent in VAF and caudal SRAF where responses were also more sharply tuned because of marked spike rate drop with increased ILD in the contralateral hemifield (Fig. 9*C*, cSRAF). Consequently, most sites in VAF and caudal SRAF were best fit with a peaked sigmoid function (Fig. 9*C*, cSRAF functions). In contrast, most sites in A1 and rostral SRAF were not peaked (Fig. 9*C*, rSRAF functions). A systematic shift in ILD tuning from caudal to rostral SRAF and from VAF to A1 allowed for a full range of best ILDs and corresponding ILD tuning (Fig. 9*C*). In theory, this distributed best ILD or maximal spike rate response to ILD could encode sound position in the sensory hemifield side opposite (contralateral) to a given cerebral hemisphere (Fig. 9*A*) as proposed previously (Bala et al., 2007). This suggests that neighboring cortical sites could compete to "capture" the most spike rate and possibly direct the animal's orientation or attention toward the position of auditory objects. Although we have not examined discrimination limits here, sites with broad ILD responses in A1 and rostral SRAF would likely require additional processing such as opponent vector summation to accurately predict sound localization behavior as suggested previously (Stecker et al., 2005b). The high degree of spike rate facilitation observed in the present study for midline ILDs in SRAF may indicate yet another mechanism for optimizing a spike rate code for sound position.

Auditory cortical ILD responses are organized according to a size-eccentricity relationship similar to that observed in other sensory modalities. Two metrics for ILD tuning, half-width and drop in spike rate, changed with best ILD, allowing for better resolution of the horizontal position cue near the midline. Spatial receptive fields are also more finely tuned for midline position-sensitive sites in cat PAF (Stecker et al., 2005b) and superior colliculus (Middlebrooks and Knudsen, 1984; Rowland et al., 2007). This may be a general feature of sensory spatial representations, as visual spatial receptive field tuning is also inversely related to horizontal eccentricity in primary and parietal belt visual cortices (Albright, 1984). In addition, binaural facilitation was highest for midline positions (i.e., ILD $<$20 dB) and was inversely related to best ILD in rostral SRAF (Fig. 8). Facilitation was not an exclusive property of sites with midline best ILDs; however, it was most pronounced for midline ILDs (Figs. 7, 8*B*). Rostral SRAF had a full range of best ILDs, and facilitation boosted the spike rate for those sites with midline best ILDs (Fig. 8*A*, green filled circles and regression line). In contrast, most caudal SRAF sites were tuned to midline ILD cues and had a significant degree of facilitation; consequently, facilitation did not change significantly with best ILD in this region (Fig. 8*A*, black filled circles). A similarly high degree of binocular facilitation has been observed at cortical sites responding maximally to visual field midline that are located at the border between primary and secondary visual cortex (i.e., area 17/18 border) (Gardner and Cynader, 1987). Thus, bilateral sensory facilitation plays a unique role in shaping narrowly tuned midline spatial cue sensitivity in both visual and auditory cortices.

According to dual stream hypotheses, mammalian cortices are specialized to discriminate distinct features including sound identity versus localization cues (Rauschecker and Tian, 2000; Romanski, 2004). Such models are supported by neural and behavioral data that compare PAF and AAF and find they specialize to process a sound's horizontal position and spectral–temporal sequence, respectively (Harrington et al., 2008; Lomber and Malhotra, 2008). Indeed, there is considerable evidence that auditory cortices and corresponding pathway inputs are specialized behaviorally, physiologically, and anatomically (Kaas and Hackett, 2000; Winer et al., 2001; Doron et al., 2002; Wallace et al., 2004; Ghazanfar and Schroeder, 2006; Polley et al., 2006, 2007,

2010; Bendor and Wang, 2008; Bizley and King, 2009; Storace et al., 2010a,b). However, a major shortcoming of current organization schemes is their failure to account for systematic organization of sound localization cue sensitivity in multiple core, belt, and parabelt auditory cortices. The present study joins several others in calling for a modified functional rubric where position cue sensitivity is a critical and ubiquitous organizational feature across multiple auditory cortices (Stecker and Middlebrooks, 2003; Harrington et al., 2008; Bizley et al., 2009; Recanzone and Cohen, 2010), similar in many respects to organization of the visual cortices (Levy et al., 2001; Hasson et al., 2002).

References

Albright TD (1984) Direction and orientation selectivity of neurons in visual area MT of the macaque. J Neurophysiol 52:1106–1130.

Bala AD, Spitzer MW, Takahashi TT (2007) Auditory spatial acuity approximates the resolving power of space-specific neurons. PLoS One 2:e675.

Bendor D, Wang X (2008) Neural response properties of primary, rostral, and rostrotemporal core fields in the auditory cortex of marmoset monkeys. J Neurophysiol 100:888–906.

Bizley JK, King AJ (2009) Visual influences on ferret auditory cortex. Hear Res 258:55–63.

Bizley JK, Walker KM, Silverman BW, King AJ, Schnupp JW (2009) Interdependent encoding of pitch, timbre, and spatial location in auditory cortex. J Neurosci 29:2064–2075.

Campbell RA, Doubell TP, Nodal FR, Schnupp JW, King AJ (2006a) Interaural timing cues do not contribute to the map of space in the ferret superior colliculus: a virtual acoustic space study. J Neurophysiol 95:242–254.

Campbell RA, Schnupp JW, Shial A, King AJ (2006b) Binaural-level functions in ferret auditory cortex: evidence for a continuous distribution of response properties. J Neurophysiol 95:3742–3755.

Chase SM, Young ED (2005) Limited segregation of different types of sound localization information among classes of units in the inferior colliculus. J Neurosci 25:7575–7585.

Clarey JC, Barone P, Imig TJ (1994) Functional organization of sound direction and sound pressure level in primary auditory cortex of the cat. J Neurophysiol 72:2383–2405.

Davis KA, Young ED (2000) Pharmacological evidence of inhibitory and disinhibitory neuronal circuits in dorsal cochlear nucleus. J Neurophysiol 83:926–940.

Doron NN, Ledoux JE, Semple MN (2002) Redefining the tonotopic core of rat auditory cortex: physiological evidence for a posterior field. J Comp Neurol 453:345–360.

Eggermont JJ (2001) Between sound and perception: reviewing the search for a neural code. Hear Res 157:1–42.

Escabi MA, Higgins NC, Galaburda AM, Rosen GD, Read HL (2007) Early cortical damage in rat somatosensory cortex alters acoustic feature representation in primary auditory cortex. Neuroscience 150:970–983.

Fuzessery ZM, Wenstrup JJ, Pollak GD (1990) Determinants of horizontal sound location selectivity of binaurally excited neurons in an isofrequency region of the mustache bat inferior colliculus. J Neurophysiol 63:1128–1147.

Gardner JC, Cynader MS (1987) Mechanisms for binocular depth sensitivity along the vertical meridian of the visual field. Brain Res 413:60–74.

Ghazanfar AA, Schroeder CE (2006) Is neocortex essentially multisensory? Trends Cogn Sci 10:278–285.

Goldberg JM, Brown PB (1969) Response of binaural neurons of dog superior olivary complex to dichotic tonal stimuli: some physiological mechanisms of sound localization. J Neurophysiol 32:613–636.

Hackett TA (2010) Information flow in the auditory cortical network. Hear Res. Advance online publication. Retrieved September 30, 2010. doi:10.1016/j.heares.2010.01.011.

Harrington IA, Stecker GC, Macpherson EA, Middlebrooks JC (2008) Spatial sensitivity of neurons in the anterior, posterior, and primary fields of cat auditory cortex. Hear Res 240:22–41.

Hartmann WH (1999) How we localize sound. Phys Today 52:24–29.

Hasson U, Levy I, Behrmann M, Hendler T, Malach R (2002) Eccentricity bias as an organizing principle for human high-order object areas. Neuron 34:479–490.

Higgins NC, Escabi MA, Rosen GD, Galaburda AM, Read HL (2008) Spectral processing deficits in belt auditory cortex following early postnatal lesions of somatosensory cortex. Neuroscience 153:535–549.

Irvine DR, Gago G (1990) Binaural interaction in high-frequency neurons in inferior colliculus of the cat: effects of variations in sound pressure level on sensitivity to interaural intensity differences. J Neurophysiol 63:570–591.

Kaas JH, Hackett TA (2000) Subdivisions of auditory cortex and processing streams in primates. Proc Natl Acad Sci U S A 97:11793–11799.

Kalatsky VA, Stryker MP (2003) New paradigm for optical imaging: temporally encoded maps of intrinsic signal. Neuron 38:529–545.

Kalatsky VA, Polley DB, Merzenich MM, Schreiner CE, Stryker MP (2005) Fine functional organization of auditory cortex revealed by Fourier optical imaging. Proc Natl Acad Sci U S A 102:13325–13330.

King AJ, Parsons CH, Moore DR (2000) Plasticity in the neural coding of auditory space in the mammalian brain. Proc Natl Acad Sci U S A 97:11821–11828.

King AJ, Bajo VM, Bizley JK, Campbell RA, Nodal FR, Schulz AL, Schnupp JW (2007) Physiological and behavioral studies of spatial coding in the auditory cortex. Hear Res 229:106–115.

Koka K, Read HL, Tollin DJ (2008) The acoustical cues to sound location in the rat: measurements of directional transfer functions. J Acoust Soc Am 123:4297–4309.

Lee CC, Winer JA (2008) Connections of cat auditory cortex: III. Corticocortical system. J Comp Neurol 507:1920–1943.

Levy I, Hasson U, Avidan G, Hendler T, Malach R (2001) Center-periphery organization of human object areas. Nat Neurosci 4:533–539.

Lomber SG, Malhotra S (2008) Double dissociation of "what" and "where" processing in auditory cortex. Nat Neurosci 11:609–616.

Macpherson EA, Middlebrooks JC (2002) Listener weighting of cues for lateral angle: the duplex theory of sound localization revisited. J Acoust Soc Am 111:2219–2236.

Middlebrooks JC, Green DM (1990) Directional dependence of interaural envelope delays. J Acoust Soc Am 87:2149–2162.

Middlebrooks JC, Knudsen EI (1984) A neural code for auditory space in the cat's superior colliculus. J Neurosci 4:2621–2634.

Middlebrooks JC, Zook JM (1983) Intrinsic organization of the cat's medial geniculate body identified by projections to binaural response-specific bands in the primary auditory cortex. J Neurosci 3:203–224.

Middlebrooks JC, Dykes RW, Merzenich MM (1980) Binaural response-specific bands in primary auditory cortex (AI) of the cat: topographical organization orthogonal to isofrequency contours. Brain Res 181:31–48.

Mrsic-Flogel TD, King AJ, Schnupp JW (2005) Encoding of virtual acoustic space stimuli by neurons in ferret primary auditory cortex. J Neurophysiol 93:3489–3503.

Mrsic-Flogel TD, Versnel H, King AJ (2006) Development of contralateral and ipsilateral frequency representations in ferret primary auditory cortex. Eur J Neurosci 23:780–792.

Musicant AD, Butler RA (1984) The influence of pinnae-based spectral cues on sound localization. J Acoust Soc Am 75:1195–1200.

Nakamoto KT, Zhang J, Kitzes LM (2004) Response patterns along an isofrequency contour in cat primary auditory cortex (AI) to stimuli varying in average and interaural levels. J Neurophysiol 91:118–135.

Nelken I, Bizley JK, Nodal FR, Ahmed B, King AJ, Schnupp JW (2008) Responses of auditory cortex to complex stimuli: functional organization revealed using intrinsic optical signals. J Neurophysiol 99:1928–1941.

Pandya PK, Rathbun DL, Moucha R, Engineer ND, Kilgard MP (2008) Spectral and temporal processing in rat posterior auditory cortex. Cereb Cortex 18:301–314.

Pollak GD, Burger RM, Park TJ, Klug A, Bauer EE (2002) Roles of inhibition for transforming binaural properties in the brainstem auditory system. Hear Res 168:60–78.

Polley DB, Steinberg EE, Merzenich MM (2006) Perceptual learning directs auditory cortical map reorganization through top-down influences. J Neurosci 26:4970–4982.

Polley DB, Read HL, Storace DA, Merzenich MM (2007) Multi-parametric auditory receptive field organization across five cortical fields in the albino rat. J Neurophysiol 97:3621–3638.

Polley DB, O'Brien B, Hackett TA, Khatri V, Kleeman K, Young M (2010) Organization and experience-dependent modification of the mouse auditory thalamocortical circuit: structure, function and behavior. Assoc Res Otolaryngol Abs:182.

Popescu MV, Polley DB (2010) Monaural deprivation disrupts develop-

ment of binaural selectivity in auditory midbrain and cortex. Neuron 65:718–731.
Rauschecker JP, Tian B (2000) Mechanisms and streams for processing of "what" and "where" in auditory cortex. Proc Natl Acad Sci U S A 97:11800–11806.
Razak KA, Fuzessery ZM (2010) GABA shapes a systematic map of binaural sensitivity in the auditory cortex. J Neurophysiol 104:517–528.
Read HL, Winer JA, Schreiner CE (2002) Functional architecture of auditory cortex. Curr Opin Neurobiol 12:433–440.
Reale RA, Imig TJ (1980) Tonotopic organization in auditory cortex of the cat. J Comp Neurol 192:265–291.
Recanzone GH (2000) Spatial processing in the auditory cortex of the macaque monkey. Proc Natl Acad Sci U S A 97:11829–11835.
Recanzone GH, Cohen YE (2010) Serial and parallel processing in the primate auditory cortex revisited. Behav Brain Res 206:1–7.
Recanzone GH, Guard DC, Phan ML (2000) Frequency and intensity response properties of single neurons in the auditory cortex of the behaving macaque monkey. J Neurophysiol 83:2315–2331.
Romanski LM (2004) Domain specificity in the primate prefrontal cortex. Cogn Affect Behav Neurosci 4:421–429.
Rowland B, Stanford T, Stein B (2007) A Bayesian model unifies multisensory spatial localization with the physiological properties of the superior colliculus. Exp Brain Res 180:153–161.
Schnupp JW, Mrsic-Flogel TD, King AJ (2001) Linear processing of spatial cues in primary auditory cortex. Nature 414:200–204.
Semple MN, Kitzes LM (1993a) Binaural processing of sound pressure level in cat primary auditory cortex: evidence for a representation based on absolute levels rather than interaural level differences. J Neurophysiol 69:449–461.
Semple MN, Kitzes LM (1993b) Focal selectivity for binaural sound pressure level in cat primary auditory cortex: two-way intensity network tuning. J Neurophysiol 69:462–473.
Sereno MI, McDonald CT, Allman JM (1994) Analysis of retinotopic maps in extrastriate cortex. Cereb Cortex 4:601–620.
Shaw EA (1966) Earcanal pressure generated by a free sound field. J Acoust Soc Am 39:465–470.
Slattery WH 3rd, Middlebrooks JC (1994) Monaural sound localization: acute versus chronic unilateral impairment. Hear Res 75:38–46.
Spezio ML, Takahashi TT (2003) Frequency-specific interaural level difference tuning predicts spatial response patterns of space-specific neurons in the barn owl inferior colliculus. J Neurosci 23:4677–4688.
Stecker GC, Middlebrooks JC (2003) Distributed coding of sound locations in the auditory cortex. Biol Cybern 89:341–349.
Stecker GC, Mickey BJ, Macpherson EA, Middlebrooks JC (2003) Spatial sensitivity in field PAF of cat auditory cortex. J Neurophysiol 89:2889–2903.
Stecker GC, Harrington IA, Macpherson EA, Middlebrooks JC (2005a) Spatial sensitivity in the dorsal zone (area DZ) of cat auditory cortex. J Neurophysiol 94:1267–1280.
Stecker GC, Harrington IA, Middlebrooks JC (2005b) Location coding by opponent neural populations in the auditory cortex. PLoS Biol 3:e78.
Storace DA, Higgins NC, Read HL (2010a) Thalamic label patterns suggest primary and ventral auditory fields are distinct core regions. J Comp Neurol 518:1630–1646.
Storace DA, Higgins NC, Read HL (2010b) Thalamocortical pathway specialization for sound frequency resolution. J Comp Neurol. Advance online publication. doi: 10.1002/cne.22501.
Tollin DJ, Koka K (2009) Postnatal development of sound pressure transformations by the head and pinnae of the cat: monaural characteristics. J Acoust Soc Am 125:980–994.
Tsai JJ, Koka K, Tollin DJ (2010) Varying overall sound intensity to the two ears impacts interaural level difference discrimination thresholds by single neurons in the lateral superior olive. J Neurophysiol 103:875–886.
Wallace MT, Ramachandran R, Stein BE (2004) A revised view of sensory cortical parcellation. Proc Natl Acad Sci U S A 101:2167–2172.
Wenstrup JJ, Fuzessery ZM, Pollak GD (1988) Binaural neurons in the mustache bat's inferior colliculus. II. Determinants of spatial responses among 60-kHz EI units. J Neurophysiol 60:1384–1404.
Wightman FL, Kistler DJ (1992) The dominant role of low-frequency interaural time differences in sound localization. J Acoust Soc Am 91:1648–1661.
Winer JA, Diehl JJ, Larue DT (2001) Projections of auditory cortex to the medial geniculate body of the cat. J Comp Neurol 430:27–55.
Zhang J, Nakamoto KT, Kitzes LM (2004) Binaural interaction revisited in the cat primary auditory cortex. J Neurophysiol 91:101–117.